3D Printing Technology in Craniofacial Surgery and Salivary Gland Regeneration

9

Jong Woo Choi, Namkug Kim, and Chang Mo Hwang

Abstract

Patient-specific three-dimensional (3D)-printed phantoms and surgical guides are being utilized more often nowadays to assist diagnosis and treatment planning for surgery, which are tailored to individual's unique needs. 3D printing surgical guides made of temporary materials can be fabricated to fit the surface of the hard or soft tissue organs by 3D modeling of the surgical interface. To date, the value of 3D printing for surgical planning as a guidance tool has been proven in various hard tissue surgical applications, such as craniofacial and maxillofacial surgery, spine surgery, cardiovascular surgery, neurosurgery, pelvic surgery, and visceral surgery. Craniofacial plastic surgery is one of the medical fields that pioneered the use of the 3D printing concept. Rapid prototyping technology was introduced to medicine in the 1990s via CAD-CAM (computer-aided design, computer-aided manufacturing). The medical models or bio-models based on the 3D printing technique represent 1:1 scale reproductions of the human anatomical region of interest that can be obtained via 3D medical imaging. The procedure for the fabrication of medical models comprises multiple steps: (1) acquisition of high-quality volumetric 3D image data of the anatomical structure to be modeled, (2) 3D image processing to extract the region of interest from the surrounding tissues, (3) mathematical surface modeling of the anatomic surfaces, (4) formatting of data for rapid prototyping, (5) model building, and (6) quality assurance of the model and its dimensional accuracy. Furthermore, tissue engineers also experience the advent of a new 3D printing era. The tissue engineering triad comprises cells, scaffolds, and growth factors. Recently, 3D technology has become sufficiently evolved to enable printing of living cells. Although

J.W. Choi, MD, PhD, MMM (✉) • N. Kim, PhD
C.M. Hwang, PhD
Department of Plastic and Reconstructive Surgery,
Department of Bioengineering, Ulsan University,
College of Medicine, Seoul, South Korea
e-mail: pschoi@amc.seoul.kr; namkugkim@gmail.com; hwang.changmo1@gmail.com

many challenging issues remain to be resolved for such complex structures, heart, kidney, and skin regenerations are being investigated using 3D bioprinting technology. A potential candidate for a clinical success resides in the regeneration of the major salivary glands, which consist of various cells encapsulated by a connective tissue membrane.

9.1 Introduction

Three-dimensional (3D) printing is a rapidly developing technology that is applied worldwide in various fields, such as business, fashion, mechanical engineering, and medicine [1, 2]. 3D printing technology has already been used in the mock formation of various products including cellular phones [2], and the extent of its applications has greatly expanded in medicine as this technology has evolved in recent years. A major advantage is that it can generate a unique product in a short period of time, which is suitable for individualized medicine where each patient requires a specific treatment, tailored to a therapeutic approach. As opposed to the products generated by 3D printing, most industrial products are mass produced, and every unit has the same dimensions. As one would expect, in the field of medicine, patients are all different in terms of any shapes and sizes that require surgical attention. The 3D printing technique supports the contemporary aim of implementing personalized medicine by providing a patient-specific product in a short period of time at reasonable prices [3].

Therefore, the clinical applications of the 3D printing technology are expanding more rapidly in recent years. The affordability and convenience of this technology have spurred its adoption in a variety of medical fields. This revolutionary technique may ultimately allow the printing of tissue and organ structures to replace damaged or missing body parts. Although outcomes and efficacy of 3D printing require more scientific research, it is clear that 3D printing technology is unique and has invaluable innovations in medicine. For example, pediatric cardiac surgeons use 3D printing-based tactile models for analyzing and visualizing complex congenital heart diseases. Urologic surgeons simulate surgery of complex renal cell carcinomas in advance of actual surgery using 3D printed tactile prototype models that include the vessels and parenchyma of the kidney. Neurosurgeons utilize similar approaches for neurosurgery of brain cancer. These types of efforts allow surgeons in various specialties to perform advanced analyses of the patient's specific status. In addition, tactile models with a real intraoperative 1:1 scale reference can be very useful for preoperative consultations with patients [3–5].

Craniofacial plastic surgery is one of the medical fields that pioneered the use of the 3D printing concept. Rapid prototype (RP) technology was introduced to medicine in the 1990s via computer-aided design and computer-aided manufacturing (CAD-CAM). The medical models or bio-models based on the 3D printing technique represent 1:1 scale reproductions of the human anatomical region of interest that can be obtained via 3D medical imaging [5]. The procedure for the fabrication of medical models comprises multiple steps: (1) acquisition of high-quality volumetric 3D image data of the anatomical structure to be modeled, (2) 3D image processing to extract the region of interest from the surrounding tissues, (3) mathematical surface modeling of the anatomic surfaces, (4) formatting of data for rapid prototyping, (5) model building, and (6) quality assurance of the model and its dimensional accuracy [3, 6].

For instance, because patients requiring craniofacial surgery tend to have very specific malformations or deformities, mostly in the bone, a 3D printing prototype model can greatly assist with preoperative evaluation and intraoperative procedures. Medical modeling in craniofacial surgery based on 3D printing has mainly been developed over the last 15 years. It can incorporate (1) aiding in the production of surgical implants, (2) improving surgical planning, (3) acting as an

orientation aid during surgery, (4) enhancing diagnostic quality, (5) assisting preoperative simulation, (6) obtaining a patient's consent prior to surgery, and (7) preparing a template for resection for surgeons as well as providing an educational tool for medical students and residents [3, 5, 7].

Meanwhile, tissue engineers also experience the advent of a new 3D printing era. The tissue engineering triad comprises cells, scaffolds, and growth factors. Recently, 3D technology has become sufficiently evolved to enable printing of living cells. Although many obstacles need to be overcome, 3D bioprinting provides bioengineers with a new modality such as 3D cell culture on scaffolds that might be superior to conventional cell culture systems. Bioprinting is an emerging technology that is expected to eventually regenerate biological tissues and even solid organs. As a combination of techniques, a nonliving scaffold could be constructed using 3D technology, while bioprinting simultaneously adds a living tissue [1, 8–12]. More specifically, tissue-compatible scaffolds are generated with bioprinting, and living cells are incorporated into them, along with various growth factors, depending on the application. Heart, kidney, and skin regenerations are being investigated using 3D bioprinting technology, although many challenging issues remain to be resolved for such complex structures. The regeneration of the major salivary glands, which consist of various cells encapsulated by connective tissue membrane, certainly requires further investigation and attention for a clinical success of 3D bioprinting. In this book chapter, the current status of 3D printing technology and its clinical applications in craniofacial surgery are reviewed. A potential application of 3D bioprinting for salivary gland regeneration is discussed at the end of the chapter.

9.2   Review of Current 3D Printing in Craniofacial Surgery (Reproduced from Ref. [28])

3D printing technology can be categorized by the techniques, the materials, or the aimed deposition process. The classification based on the techniques includes stereolithography (SL), selective laser sintering (SLS), 3D printing (3D printer-based SLS: 3DP), fused deposition modeling (FDM), direct metal laser sintering (DMLS), laminated object manufacturing (LOM), and electron beam melting (EBM). The materials used for the 3D printing technology include thermoplastic, metal powder, ceramic powder, eutectic metals, alloy metal, photopolymer, paper, foil, plastic film, and titanium alloys. The 3D technology can be classified by the aimed deposition process. PolyJet modeling and 3D plotting technology are based on drop-on-drop deposition. 3D printing is based on drop-on-powder deposition. Fused deposition modeling is based on continuous deposition. The most frequently used representative methods are reviewed and summarized in Table 9.1 [3].

9.2.1   Liquid-Based 3D Printing Technology

9.2.1.1   Stereolithography (SL or SLA)

Stereolithography (SL) has been the most widely used 3D printing technique for craniofacial surgery since it was first applied for grafting a skull defect in 1994 [13]. The SL RP system consists of a bath of photosensitive resin, a model-building platform, and an ultraviolet (UV) laser for curing the resin. A mirror is used to guide the laser focus onto the surface of the resin; the resin becomes cured when exposed to the UV radiation. The mirror is computer controlled and is guided to cure the resin on a slice-by-slice basis. These slice data are fed into the RP machine that directs the exposure path of the UV laser onto the surface of the resin. The layers are cured sequentially and bind together to form a solid object, beginning from the bottom of the model and building upward. Each new layer of resin is wiped across the surface of the previous layer using a wiper blade before being exposed and cured. The model is then removed from the bath and cured for an additional period of time in a UV cabinet. [14].

Generally, SL is considered to provide the greatest accuracy and best surface finish of any

Table 9.1 A comparison of current 3D printing technologies

	3D printing technology	Materials	Aimed deposition process
Liquid base	SL (Stereolithography)	Photopolymer	
	Polyjet or Multijet Printing	ABS, Acryl	Drop-on-drop deposition
Powder base	SLS (Selective Laser Sintering)	Thermoplastics	
		Metal powder	
	3DP (3D printing)	Plastic powder	Drop-on-powder deposition
	DMLS (Direct Metal Laser Sintering)	Alloy metal	
		Ceramic powder	
	EBM (Electron beam melting)	Titanium alloys	
Solid base	FDM (Fused Deposition Modeling)	Thermoplastics	Continuous deposition
		Eutectic metals	
		ABS	
	LOM (Laminated object manufacturing)	Paper	
		Foil	
		Plastic film	

Reprinted from ref [18]. ABS, acrylonitrile butadiene styrene

RP technology. The model material is robust, slightly brittle, and relatively light [15]. SL accuracy is 1.2 mm (range, 0–4.8 mm) for skull base measures, 1.6 mm (range, 0–5.8 mm) for midface measures, 1.9 mm (range, 0–7.9 mm) for maxilla measures, and 1.5 mm (range, 0–5.7 mm) for orbital measures. The mean differences in defect dimensions are 1.9 mm (range, 0.1–5.7 mm) for unilateral maxillectomy, 0.8 mm (range, 0.2–1.5 mm) for bilateral maxillectomy, and 2.5 mm (range, 0.2–7.0 mm) for orbitomaxillectomy defects [16]. Midface SL models may be more prone to error than those of other craniofacial regions because of the presence of thin walls and small projections. Choi et al. [29] found that the absolute mean deviation between an original dry skull and an SL RP model over 16 linear measurements was 0.62 ± 0.5 mm (0.56 ± 0.39 %) [15, 17]. The accuracy of computed tomography (CT) and SL models was compared. The accuracy for SL models expressed as the arithmetic mean of the relative deviations ranged from 0.8 to 5.4 %, with an overall mean deviation of 2.2 %. The mean deviations of the investigated anatomical structures ranged from 0.8 to 3.2 mm. An overall mean deviation (comprising all structures) of 2.5 mm was found.

9.2.1.2 PolyJet Modeling

PolyJet modeling is performed by jetting state-of-the-art photopolymer materials in ultrathin layers (16 μm) onto a build tray layer by layer until the model is completed. Each photopolymer layer is cured by UV light immediately after it is jetted, producing fully cured models that can be handled and used immediately without post-curing. The gel-like support material used, which is specially designed to support complicated geometries, is easily removed by hand and water jetting [14]. At present, this technique is too time-consuming and expensive to be used in craniofacial surgery clinical applications. Ibrahim et al. reported a dimensional error of 2.14 % in reproducing a dry mandible when using this technique [18].

9.2.2 Powder-Based 3D Printing Technology

9.2.2.1 Selective Laser Sintering (SLS)

The selective laser sintering (SLS) technique uses a CO_2 laser beam to selectively fabricate models in consecutive layers. First, the laser beam scans over a thin layer of powder previously deposited on the build tray and leveled with a roller. The laser heats the powder particles, fusing them to form a solid

layer, and then moves along the x- and y-axes to design the structures according to the CAD data. After the first layer fuses, the build tray moves downward, and a new layer of powder is deposited and sintered, and the process is repeated until the object is completed. The prototype surface is finished by sandblasting [14]. The SLS prototype is opaque, and its surface is abrasive and porous. Prototype fabrication time is 15 h. The accuracy of the SLS model is relatively high, with maximum standard errors of 0.1–0.6 mm. This accuracy depends on the thickness of the CT scans used, which should be as thin as possible (1–2 mm is a good compromise for a skull study). Because of the high cost of the materials, several parts are fabricated simultaneously. The long fabrication time for the SLS technique (16 h) is close to the time required for fabrication with the SL system [19].

9.2.2.2 3D Printer-Based SLS (3D Printing)

The 3D printing system uses a print head to selectively disperse a binder onto powder layers. This technology has a lower cost than similar techniques. First, a thin layer of powder is spread over a tray using a roller similar to that used in the SLS system. The print head scans the powder tray and delivers a continuous jet of a solution that binds the powder particles as it touches them. No support structures are required while the prototype is being fabricated because the surrounding powder supports the unconnected parts. When the process is complete, the surrounding powder is aspirated. In the finishing process, the prototype surfaces are infiltrated with a cyanoacrylate-based material to harden the structure [19]. The printing technique enables the formation of complex geometrical structures, such as hanging partitions inside the cavities, without artificial support structures [14].

After the CT scan, the rendering of the DICOM data and transformation into STL data files take a maximum of 30 min, and the printing and infiltration process takes approximately 4–6 h. Simpler models can be purchased for as little as $300–$400 [19]. The 3D printers used in this process are relatively inexpensive ($2500–$3000), have fast build times (4 h for a full skull), and are easy to maintain. Additionally, 3D printers are cost-effective,

associated with low waste, and accurate (± 0.1 mm in the Z plane, ± 0.2 mm in the X and Y planes), and they can make hard, soft, or flexible models. These printers can also be used to identify different types of body tissue depending on the predefined threshold setting selected. Silva et al. reported a mean dimensional error of 2.67 % in prototypes produced using 3D printing technologies in comparison with a dry human skull [19].

9.2.3 Solid-Based 3D Printing Technology

9.2.3.1 Fused Deposition Modeling

Fused deposition modeling (FDM) uses a similar principle to SL in that it builds models on a layer-by-layer basis. The main difference is that the layers are deposited as a thermoplastic that is extruded from a fine nozzle. A commonly used material for this procedure is acrylonitrile butadiene styrene (ABS). The 3D model is constructed by extruding the heated thermoplastic material onto a foam surface along a path indicated by the model data. Once a layer has been deposited, the nozzle is raised between 0.278 and 0.356 mm, and the next layer is deposited on top of the previous layer. This process is repeated until the model is completed [14]. As with SL, support structures are required for FDM models because time is needed for the thermoplastic to harden and the layers to bond together [20].

9.3 Patient-Specific Modeling and Its Clinical Application Using 3D Printing Technology

9.3.1 Patient-Specific Modeling from Medical Images and Computer-Aided Design

As depicted in Fig. 9.1, after patient scanning with CT and/or MRI, the DICOM data can be transferred and processed into STL data files or other 3D file formats by using segmentation, surface extraction, and 3D model post-processing. Less than a 1-mm CT slice thickness and voxel with iso-
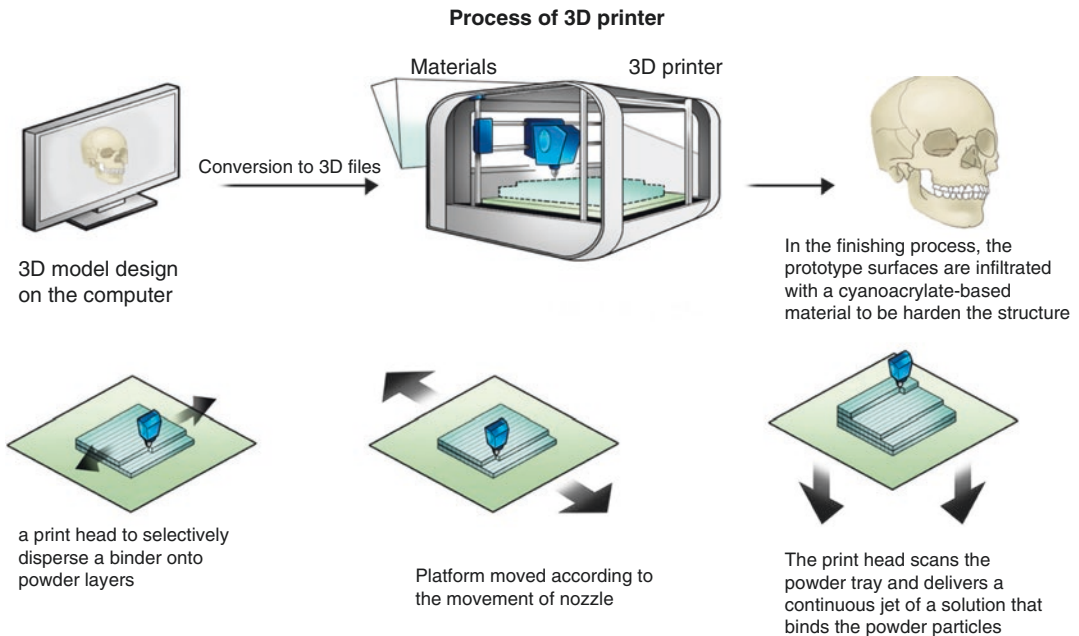
Process of 3D printer

Materials   3D printer

Conversion to 3D files

3D model design
on the computer

In the finishing process, the
prototype surfaces are infiltrated
with a cyanoacrylate-based
material to be harden the structure

a print head to selectively
disperse a binder onto
powder layers

Platform moved according to
the movement of nozzle

The print head scans the
powder tray and delivers a
continuous jet of a solution that
binds the powder particles

Fig. 9.1 The overall process of 3D printing in craniofacial surgery. After the patient is scanned via CT, DICOM files should be exported. Less than a 1-mm CT slice thickness is recommended. DICOM data are imported and converted to stereolithography (STL) files. Rendering of CT scan DICOM data into STL data files takes about 30 min. Converted 3D files are uploaded into the 3D printer. Rapid prototyping (RP) uses layer-by-layer stereolithographic accumulation. The RP model is then fabricated on plaster via jetting of a material that consists of plaster (<90 %), vinyl polymer (<20 %), and carbohydrate (<10 %). The printing and infiltration process takes about 4–6 h. Finally, unsintered sections are removed (Reprinted from Ref. [18])

cubic spacing are recommended. The time required mainly rests on the clinical application. In particular, segmentation is a critical procedure for improving the overall accuracy and needs considerable time. No satisfactory fully automated medical image segmentation algorithms have been established. Therefore, manual or semiautomated segmentation algorithms have generally been used, which have enhanced the importance of operator experience. After segmentation, a surface model should be produced by a marching cube [21, 22] or other 3D contour extraction algorithms [23]. For medical visualization, these kinds of shaded surface display techniques are well established. However, this 3D model by itself is not good enough for 3DP, due to, for example, too many mesh units and incomplete topological soundness. Therefore, topological correction [24], decimation [25], Laplacian smoothing [26], and local smoothing [27] are required to make a 3D model for 3DP. In addition, virtual simulation, including determination of the entry point and direction of the screw and surgical line, is accomplished for patient-specific

surgical planning. Based on this planning, surgical guides are designed by computer-aided design (CAD) software. After the generation of a 3D model, the most suitable 3D printer for their applications is selected among various kinds of 3DP techniques. The 3D model file is uploaded into the 3D printer. The 3D printer uses layer-by-layer STL accumulation to fabricate the 3D physical model.

9.3.2 Applications for Personalized Treatment

9.3.2.1 Surgical Planning and Guidance Tools

Patient-specific 3D printed phantoms and surgical guides are being used more often to aid diagnosis and treatment planning for surgery, which allow individual customization. 3D printing surgical guides made of temporary materials can be fabricated to fit the surface of the hard or soft tissue organs by 3D modeling of the surgical interface. To date, the value of 3D printing for surgical

planning as a guidance tool has been proven in various hard tissue surgical applications, such as craniofacial and maxillofacial surgery [28–33], spine surgery [34], cardiovascular surgery [35, 36], neurosurgery [37, 38], pelvic surgery [39, 40], and visceral surgery [41].

Recent advances in 3D printable materials have increased the level of realism of the 3D phantoms used for surgical planning. Improved diversity due to better transparency, color, and softness facilitates better understanding of complex 3D anatomical structures and guidance functions for soft tissues [42]. Yang et al. [43] used a full-colored and flexible 3D printed phantom as a preplanning simulator for extended septal myectomy. From the cardiac CT data, a myocardial 3D model was made by in-house software (A-view Cardiac; Asan Medical Center, Seoul, Republic of Korea). Using a 3D printer (Connex3 Objet500; Stratasys Corporation, Rehovot, Israel), the left ventricular (LV) myocardium, papillary muscle, and intraventricular muscle band (including the accessory papillary muscle) were fabricated with differently colored materials, whose flexibility could be controlled by adding a rubberlike and transparent material (Fig. 9.1). The 3D printed phantom provided invaluable information on the LV geometry. It is known that the softest 3D printable materials cannot be directly used as surgical simulators because they are still too hard for scalpel incision and suturing. Therefore, additional post-processing using gelatin or silicone molding techniques or a novel 3D printing system that can directly jet a variety of silicone materials needs to be developed.

9.3.2.2 Implantable Devices

3D printing techniques are also used in implant design to make patient-specific prosthetics, outside the standard range of ready-made commercial implants (Fig. 9.2). In addition, this approach has improved surgical performance by enabling the creation of patient-specific anatomy-based implants. For hard tissue structures, metal implants have, in particular, been successfully used in various applications [44, 45], which were mostly FDA cleared, such as mandible [33] and dental [46] restoration and hip [47], femoral [48], and hemi-knee joint reconstruction [44, 45]. In
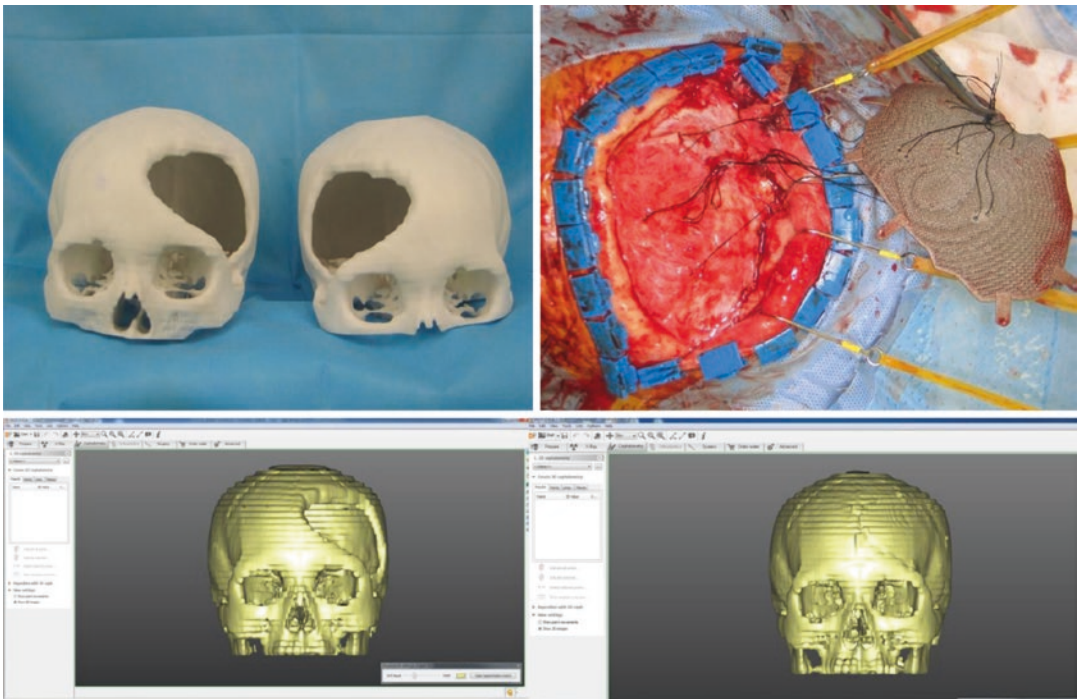

Fig. 9.2 Large cranial defect reconstructed with 3D printed titanium implant. *Top panels*: The contralateral normal cranium was mirrored and the 3D printed titanium implant was inserted for the correction of the calvarial bone defect (Modified from Ref. [18]). *Bottom panel*: Computer-simulated skull defect images before (*left*) and after (right) titanium implant was inserted

addition, the biocompatible ceramic hydroxyapatite [49] and the biodegradable polymer polycaprolactone [50] have been used in 3D printing-based applications to substitute hard tissues with customized implants.

Beyond the hard tissue applications, customized implants created using 3D printing have recently been used in the interventional field. Amerini et al. [51] revealed the feasibility of a personalized interventional treatment for tricuspid regurgitation using a braided stent in an animal study. From the cardiac CT data, the 3D reconstructed model of the right-sided cardiac cavities of a pig was obtained (OsiriX® Imaging Software; Pixmeo, Switzerland). A solid Alumide® mold was manufactured using a 3D printing system, and then a personalized compressible nitinol stent was subsequently produced and fitted onto the 3D printing mold (Fig. 9.3). This customized stent was almost completely fitted onto the right atrium,
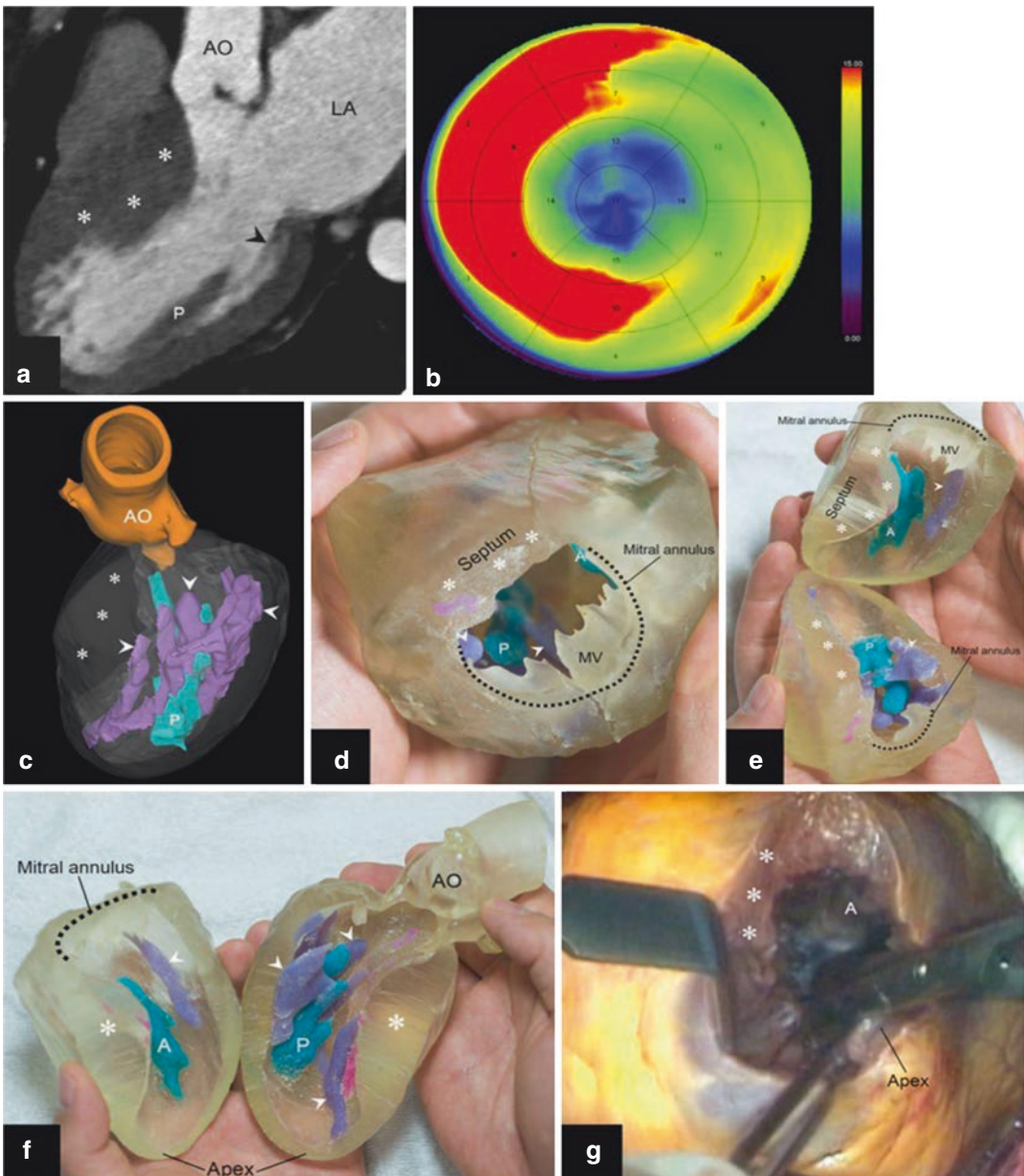
and an additional tubular stent component containing a tissue valve prosthesis was established. In the feasibility study performed in animals, they found that the 3D printing-based stent could stabilize the biological valve prostheses by force transmission from the annulus to the atrial wall and the adjacent vena cava.

In this book chapter, only clinical applications with previously developed 3D printing technologies were discussed. However, other approaches for personalized implants have been proposed, including bioprinting of tissues and organs [52–54] and the organ-on-a-chip technique [55, 56].
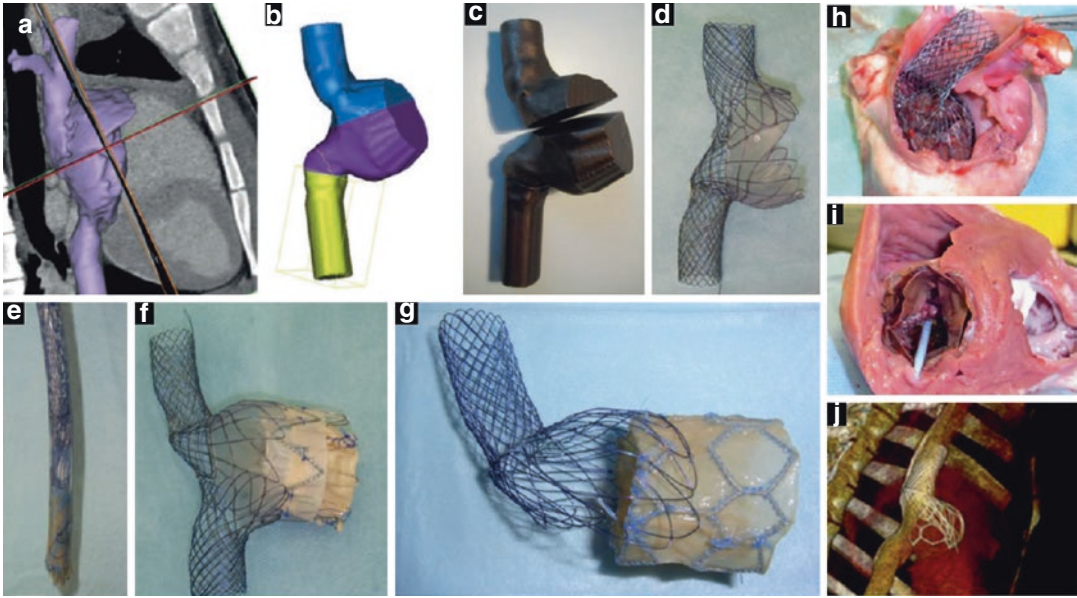

Fig. 9.4 In silico tridimensional reconstruction of the right-sided cardiac cavities of a female pig. (**a**) CT-based primary 3D reconstruction. (**b**) 3D reconstructed model of main structural parts. (**c**) 3D printed phantom mold of the main structural parts with alumide material. (**d**) A personalized stent with nitinol material. (**e**) An equipped state of the developed stent in an introducer. (**f, g**) Two different types of the prototype equipped with a self-expanding bioprosthetic valve. (**h, j**) Study results [51] showing implantation of the developed stent. Postmortem autopsy (h, i) and CT fluoroscopy (j) both revealed accurate positioning of the valve prostheses (Reproduced from Ref. [51])

Fig. 9.3 A cardiac three-chamber CT image and 3D printing of the heart. (**a**) CT imaging demonstrating a hypertrophied interventricular septum (*asterisks*), posterior papillary muscle (*P*), and intraventricular muscle band or accessory papillary muscles (*arrowhead*). (**b**) A bull's-eye map generated by using the end-diastolic phase of the CT imaging shows the extent of the hypertrophied myocardium (*red area*, >15 mm in thickness). (**c**) 3D reconstructed model. (**d–f**) 3D printed phantom of the myocardium showing the geometric relationship among the hypertrophied septum (*asterisks*), papillary muscle (*A* anterior, *P* posterior), and intraventricular muscle band (*asterisks*). (**g**) Intraoperative photography via the apical approach shows the limited visual field of the LV cavity. The base of the anterior papillary muscle is exposed after excision of the muscle band (not shown) near the anterior papillary muscle. *LV* left ventricle (Reprinted from Ref. [43])
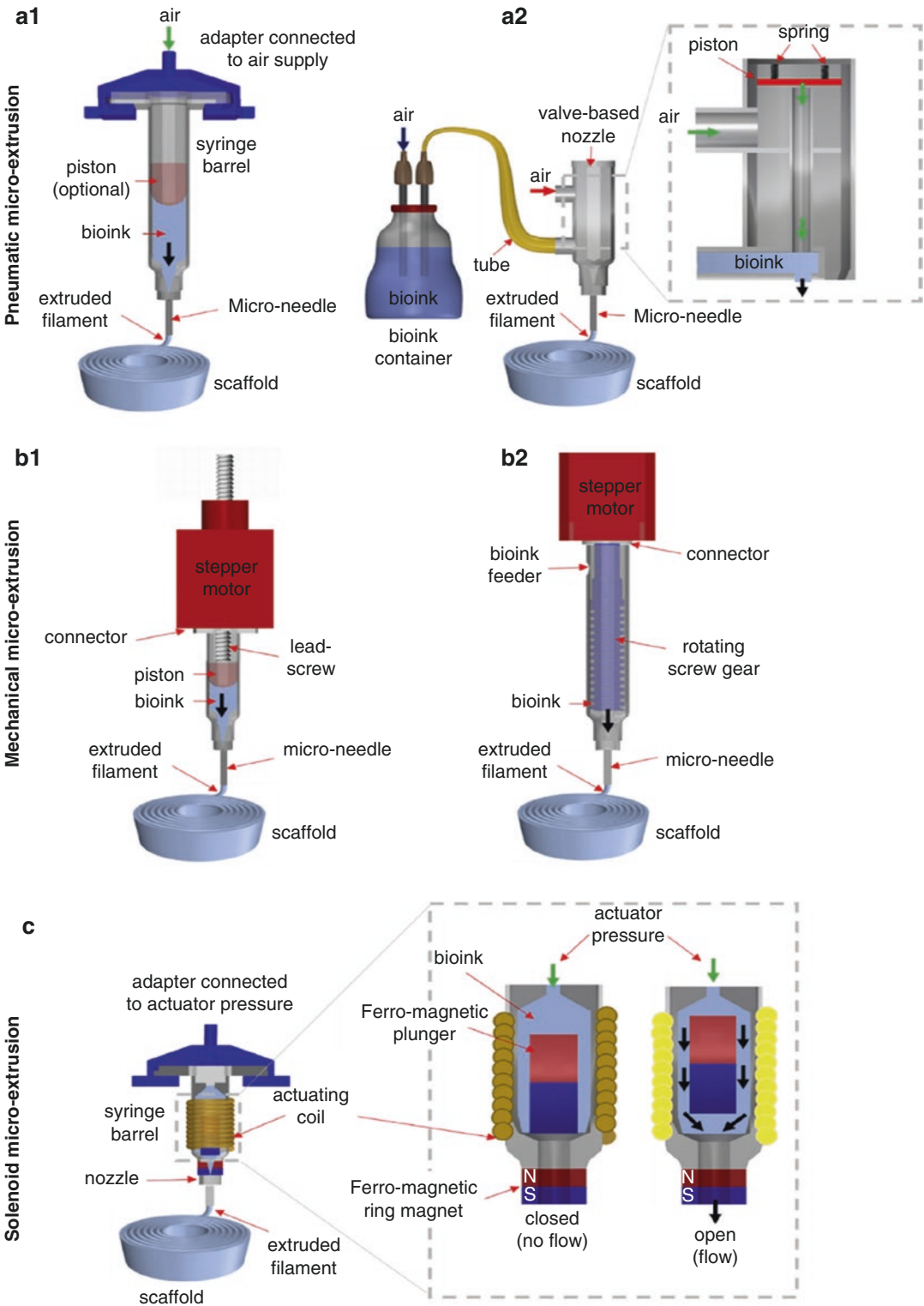
a1

Pneumatic micro-extrusion

air

adapter connected
to air supply

syringe
barrel

piston
(optional)

bioink

extruded
filament

Micro-needle

scaffold

a2

piston

spring

air

valve-based
nozzle

air

air

bioink

bioink
container

tube

extruded
filament

Micro-needle

scaffold

b1

Mechanical micro-extrusion

stepper
motor

connector

lead-
screw

piston

bioink

extruded
filament

micro-needle

scaffold

b2

stepper
motor

bioink
feeder

connector

rotating
screw gear

bioink

extruded
filament

micro-needle

scaffold

c

Solenoid micro-extrusion

adapter connected
to actuator pressure

syringe
barrel

actuating
coil

nozzle

extruded
filament

scaffold

actuator
pressure

bioink

Ferro-magnetic
plunger

actuator pressure

Ferro-magnetic
ring magnet

N
S

closed
(no flow)

N
S

open
(flow)

Fig. 9.5 Extrusion-based bioprinting systems: (**a**) pneumatic micro-extrusion including valve-free (*A1*) and valve based (*A2*) and (**b**) motor-driven micro-extrusion includ-ing piston (*B1*) and screw-driven (*B2*) and (**c**) solenoid micro-extrusion (Reprinted from Ref. [71])
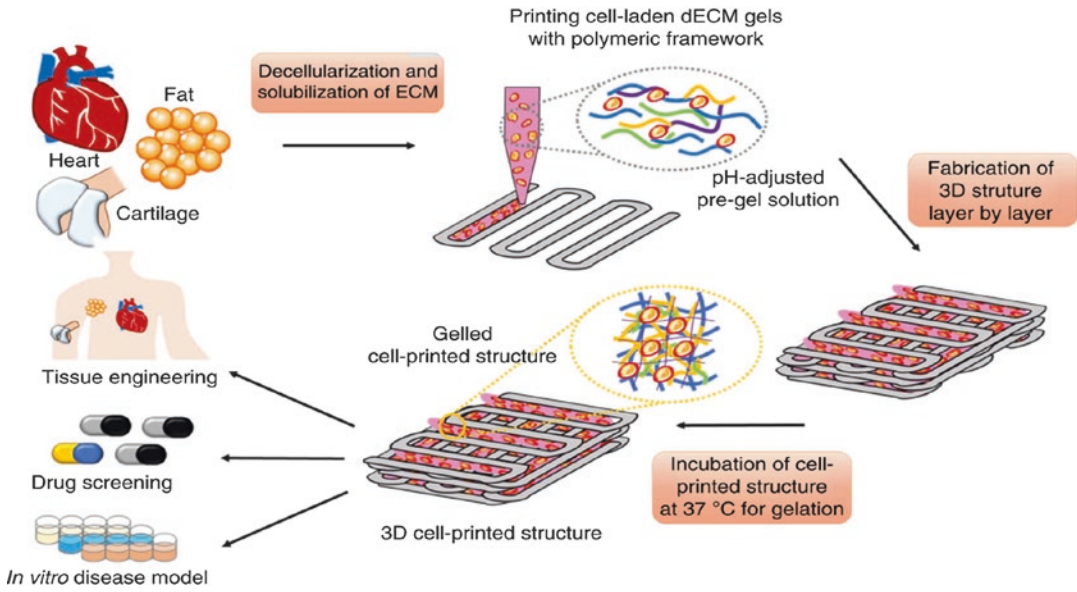
Fig. 9.6 Extrusion bioprinting with tissue originated bioinks. Biodegradable synthetic polymer scaffold is coextruded side by side to hydrogel bioink to maintain 3D architecture of printed objects (Reprinted from Ref. [70])
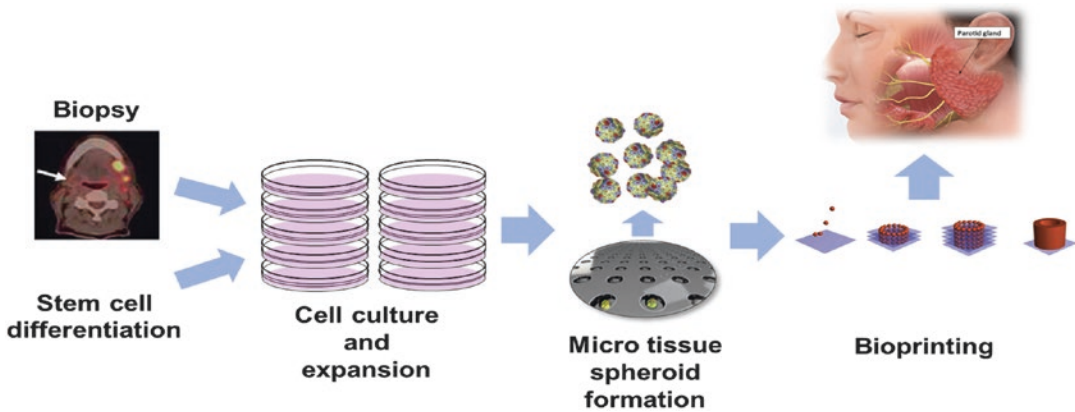

Fig. 9.7 Salivary gland regeneration with microsphere 3D bioprinting (Reproduced from Refs. [82, 88])

9.4   3D Bioprinting and Salivary Gland Regeneration

9.4.1   3D Bioprinting Considerations

An increasing number of publications for 3D bioprinting report significant progress and successes in vitro and in vivo. The three major components of tissue engineering include cells, scaffolds, and biological factors that facilitate tissue growth and organization. Similarly, key elements of bioprinting consist of cells, bioprinter, bioink, and the bioreactor system. The choice of cells for tissue reconstruction depends on the types of cells in the target tissues and organs. For example, vascular endothelial cells and smooth muscle cells would be appropriate for blood vessel printing and fibroblasts for connective tissues. Stem cells are frequently considered as a potential source of cells as well.

The selection of cell types has been widely investigated in the tissue engineering literature [57–61]. Therefore, it will not be explained further here. Bioreactors can be employed for the maturation of printed tissue constructs into functional tissue units and organs [62–64]. Generally, bioprinted three-dimensional tissue constructs are formed layer by layer by printing bioinks that contain living cells. Current 3D bioprinting research mainly focuses on the printing device and material compositions. The two most widely employed bioprinting mechanisms would be the inkjet printing and extrusion printing [65].

9.4.1.1 Inkjet Printing

Inkjet printing has a mechanism which is very similar to conventional office inkjet printers, with serial deposition of cell-containing bioink droplets. Piezoelectric actuators, heat-assisted bubble jet actuators, and pneumatic pressurization with solenoid valves are examples of inkjet printing techniques used to generate droplets [66–68]. The electronic control system of inkjet bioprinters enables relatively precise cell positioning, which can be used for drug testing or small-scale tissue unit fabrication.

9.4.1.2 Extrusion Printing

Extrusion-based printing is the most widely used bioprinting system [57, 69, 70]. Cell-containing material (bioink) is extruded from a reservoir to the printing bed through printer nozzles as shown in Fig. 9.5. The driving mechanism of extrusion can be pneumatic pressure or motor-driven syringe plunger movement [70, 71].

9.4.1.3 Bioinks

Cell behaviors including adhesion, migration, proliferation, differentiation, and tissue formation are influenced by the extracellular microenvironments, both in vivo and in vitro. After printing, cells are encapsulated in the bioink, and cell behavior is mainly affected by the biophysicochemical properties of the bioink, such as stiffness, molecular structure, cytokines or growth factors, degradability, and permeability [71–73].

The first consideration of materials as a bioink is printability. An appropriate shape holding mechanism is necessary to maintain 3D configuration of printed objects. The transition of bioinks from liquid to solid (semisolid) should be shorter than significant shape change. The stability of bioprinted constructs mainly depends on the viscosity of the bioinks after printing.

Liquid phase bioinks out of the printer nozzle are subject to surface tension and gravitational force. These external forces affect shape change of printed bioinks until possessing high enough viscosity.

From the viscosity point of view, materials with short cross-linking time can be a first consideration as bioink candidates. Bioink materials modified to have a short gelling time are widely used in 3D bioprinting. Hydrogels with short cross-linking time are widely employed as bioinks because these materials have dimensional stability in a relatively short time after printing [65, 66, 69, 74, 75].

Another approach for high viscosity is employing thixotropic materials to improve the stability of printed 3D constructs during cross-linking. Thixotropic materials are usually semi-solid and have a shear thinning property (thixotropic means "shear thinning"). During bioink printing through the printer nozzle, shear forces induce a lowering of the viscosity, and bioinks have low flow resistance, with minimal harmful effect to the suspended cells. After exiting the nozzle, the thixotropic materials regain their high viscosity, and shape changes are minimized [76]. This prevents the collapse of printed 3D constructs.

One additional advantage of thixotropic bioink is the absence of cell sedimentation in the reservoir during the printing process. As the specific gravity of a cell is slightly higher than water, suspended cells tend to localize on the bottom of a reservoir. This effect is significant when cells are suspended in a low viscosity liquid. In thixotropic bioinks, suspended cells may show no or negligible displacement. As printing time is proportionally increased with the volume of an object, inhomogeneous cell distribution

would be a significant defect in human-sized organs made with non-thixotropic aqueous bioinks. While extruding with thixotropic bioinks, care must be taken to keep the proper shear stress range to avoid lowering suspended cell viability. In side-by-side polymer printing the nonporous structure of each layer can be employed as a supporting structure to improve dimensional stability of constructs during 3D bioprinting as shown in Fig. 9.6 [57, 70, 77, 78].

Hydrogels can provide cells with a minimum damage environment during the bioprinting process. Hydrogels are widely used as a bioink material with a cell compatible pH and appropriate osmolarity. Examples of biomaterials with natural origins are alginate, fibrin, gelatin, hyaluronic acid, and collagen, and synthetic biomaterials are polyethylene glycol and Pluronic® F-127 [70, 72–74, 78]. Mixtures of these materials are also used with optimized printability, low cell damage, and higher 3D printed construct stability.

The cross-linking mechanism depends on hydrogels' intrinsic characteristics. Alginate has ionically cross-linking, and simple contact of alginate solution with divalent cationic solutions, such as calcium, barium, and strontium, can generate cross-linked hydrogel. Due to its low cost and simple cross-linking process, alginate is often employed as an initial test material for various bioprinters. Collagen and decellularized extracellular matrix (dECM) have pH- and temperature-dependent cross-linking manner [57, 70, 74, 77]. Under the physiologic pH condition and temperature (pH 7.4 and 37 °C, respectively), these materials cross-link to form stable hydrogel matrix. Further, with high cytocompatibility, cells in collagen and dECM show high tissue formation superior to alginate. However, relatively long cross-linking time (~30 min under 37 °C) hampers widespread use of these materials as bioink [57, 75]. Fibrin has enzyme-activated cross-linking mechanism. By mixing fibrinogen solution with thrombin solution, a stable fibrin hydrogel forms. Fibrinogen is a blood coagulation protein and has high cytocompatibility but still has relatively longer cross-linking time (0.5~10 min) than alginate (0.5~5 s).

Photo-cross-linking polymers are also being widely investigated as bioinks. Hydrogel precursors, including methacrylated gelatin (GelMA), star poly(ethylene glycol-co-lactide)-acrylate (SPELA), poly(ethylene glycol) dimethacrylate (PEGDMA), and polyethylene glycol) diacrylate (PEGDA), can be cross-linked using UV light [73, 79, 80]. A brief summary of bioinks currently used are listed in Table 9.2. Bioink materials that support cell viability and proliferation and have short cross-linking time are still needed to be developed for employing 3D bioprinting process for tissue regeneration. Bioprinters should have appropriate design compatible to bioink's cross-linking mechanism. Dual or multiple mixing nozzle configuration is required for mixing precursor solutions. Cooling or heating temperature control should be considered for temperature-induced cross-linking materials [80, 81].

9.4.2 Salivary Gland Regeneration by 3D Bioprinting

The ultimate goal of 3D bioprinting is to provide vascularized functional living organs, which can be applied to the replacement of missing or disabled tissues and organs. Observations and lessons from developmental biology can provide fundamental and practical ideas for tissue engineering approaches. Specific tissues or organs at different stages of development will have varying structural requirements. The essential morphogenetic steps and events of organogenesis during developmental stage can provide insights for salivary gland regeneration through 3D bioprinting [82].

Salivary glands consist of saliva-secreting acinar cells and various other types of cells. Tissue engineering of salivary glands was tried with several different approaches with hydrogel material for tissue regeneration [83–85]. Tissue spheroids, which have been used as an in vitro 3D model system in biomedical and tumor research for several decades, may be a useful candidate in salivary gland regeneration with 3D bioprinting technology (Fig. 9.7) [77, 82].

Table 9.2 Hydrogels used in extrusion-based bioprinting

Hydrogel type	Bioink	Cross-linking mechanism in extrusion bioprinting	Solidification reversibility	Extrusion bioprinting system	Advantages	Disadvantages
Alginate	Aggregates, proteins, encapsulated cells (skeletal myoblasts, BMSC, SMC, MSC, ASC, CPC, chondrocytes, cardiomyocytes)	Ionic	–	Pneumatic micro-extrusion and bioplotter	Biocompatibility, good extrudability and bioprintability, fast gelation, good stability and integrality of printed construct, medium elasticity, low cost, nonimmunogenic	Low cell adhesion and spreading without modification of hydrogel
Collagen type I	Encapsulated cells (bovine aortic endothelial cells, keratinocytes, fibroblasts, rat neural cells, MSC, AFS)	pH mediated or thermal	–	Pneumatic micro-extrusion	Cell adherent, promote proliferation, signal transducer, good extrusion and bioprinting abilities, nonimmunogenic	Poor mechanical properties, slow gelation, unstable
Gelatin	Encapsulated cells (HepG2, hepatocytes, fibroblasts, SMC)	Thermal	+	Mechanical and pneumatic micro-extrusion	Cell adherent, biocompatible, nonimmunogenic	Unstable, fragile, weak mechanical properties at physiological temperature and low abilities to extrude and print without modification
PEG	Encapsulated cells (bone marrow stem cells or porcine aortic valve interstitial cells)	Ionic, physical, or covalent agents	–	Pneumatic micro-extrusion	Support cell viability, biocompatible, nonimmunogenic, widely used in tissue engineering when modified	Low proliferation rate, low cell adhesion, weak mechanical properties and stability without modification
Fibrin	Acellular scaffolds or encapsulated cells (AFS, HUVEC)	Enzymatic	–	Pneumatic micro-extrusion	Promote angiogenesis (causes inflammatory response), fast gelation, good integrality, medium elasticity	Difficult to control geometry, low mechanical properties, limited EBB printability

Material	Cells	Crosslinking	+/−	Advantages	Printing method	Disadvantages
Matrigel	Encapsulated cells (HepG2, BMSCs, gMSC, gEPC)	Thermal	−	Promote cell differentiation and vascularization of construct, support cell viability, good bioprintability, highly suitable particularly for cardiac tissue engineering	Pneumatic micro-extrusion	Slow gelation, which affects mechanical stability, requires cooling system for extrusion bioprinting, expensive
Agarose	Encapsulated cells (BMSCs osteosarcoma cells, MSC)	Thermal	+	High mechanical properties, stable, resistant for protein adsorption, low cost, good integrality, nonimmunogenic	Pneumatic and mechanical micro-extrusion	Low cell adhesion, fragile, require heating system for extrusion bioprinting
Chitosan	Acellular scaffolds, encapsulated cells (cartilage progenitor cells, MSC, CPC)	Ionic or covalent agents	−	Antibacterial and antifungal, medium printability, nonimmunogenic	Pneumatic micro-extrusion	Weak mechanical and stability properties without modification, slow gelation rate
Pluronic® F-127	Encapsulated cells (human primary fibroblasts, BMSC, HepG2)	Thermal	+	High printability, good bioprintability, nonimmunogenic	Pneumatic and mechanical micro-extrusion	Poor mechanical and structural properties, slow gelation, rapid degradation, require heating system for extrusion bioprinting
Hyaluronic acid	Encapsulated cells (chondrocytes, HepG2, C3A, fibroblasts)	Ionic, covalent agents	−	Promote proliferation and angiogenesis, fast gelation, good bioprintability, nonimmunogenic	Pneumatic and mechanical micro-extrusion	Rapid degradation, poor mechanical properties and low stability without modification
Methylcellulose	Encapsulated chondrocytes	Thermal, pH mediated	+	High printability, nonimmunogenic	Mechanical micro-extrusion	Low bioprintability, sensitive on common cell culture media, unstable

Reprinted from Ref. [71]

Bioprinting, or robotic additive biomanufacturing, could be implemented by a precise layer-by-layer placement of self-assembled tissue spheroids in advanced hydrogels. The rapid process of tissue spheroids to self-assemble and to form mature tissue in a relatively short time scale may provide the versatility needed for successful 3D bioprinting. Advancement of the tissue spheroids-based approach demands the synthesis of sophisticated soft biomaterials and extracellular matrices, such as bio-processible and biomimetic stimuli-sensitive functional hydrogels as bioink materials [71].

Salivary gland regeneration is also possible using 3D bioprinting with cells and hydrogels. Cells in the duct close to the acini are believed to provide all the cell types required for the formation of acini and ducts. In vitro cultured salivary cells could be assembled into three-dimensional acinar and ductal structures in the presence of collagen and Matrigel® [86]. Bioprinting of three-dimensional salivary gland structures may be guided by present experience with 3D bioprinting of vascular branch formation [72, 87]. Advancement in 3D bioprinting technology, in combination with a fundamental understanding of the molecular mechanisms of development, provides a novel strategy for salivary gland regeneration.

Conclusions

3D printing technology enables more effective patient consultations, increases diagnostic quality, improves surgical planning, acts as an orientation aid during surgery, and provides a template for surgical resection. In addition, as bioprinting technology further evolves, tissues or organs might one day be made with patient-specific shapes and dimensions, thus substantializing the goal of individualized medicine.

References

1. Müller A, Krishnan KG, Uhl E, Mast G. The application of rapid prototyping techniques in cranial reconstruction and preoperative planning in neurosurgery. J Craniofac Surg. 2003;14(6):899–914.

2. Poukens J, Haex J, Riediger D. The use of rapid prototyping in the preoperative planning of distraction osteogenesis of the cranio-maxillofacial skeleton. Comput Aided Surg. 2003;8(3):146–54.

3. Wagner JD, Baack B, Brown GA, Kelly J. Rapid 3-dimensional prototyping for surgical repair of maxillofacial fractures: a technical note. J Oral Maxillofac Surg. 2004;62(7):898–901.

4. Faber J, Berto PM, Quaresma M. Rapid prototyping as a tool for diagnosis and treatment planning for maxillary canine impaction. Am J Orthod Dentofacial Orthop. 2006;129(4):583–9.

5. Mavili ME, Canter HI, Saglam-Aydinatay B, Kamaci S, Kocadereli I. Use of three-dimensional medical modeling methods for precise planning of orthognathic surgery. J Craniofac Surg. 2007;18(4):740–7.

6. D'Urso PS, Effeney DJ, Earwaker WJ, Barker TM, Redmond MJ, Thompson RG, et al. Custom cranioplasty using stereolithography and acrylic. Br J Plast Surg. 2000;53(3):200–4.

7. Paiva WS, Amorim R, Bezerra DAF, Masini M. Aplication of the stereolithography technique in complex spine surgery. Arq Neuropsiquiatr. 2007;65(2B):443–5.

8. Armillotta A, Bonhoeffer P, Dubini G, Ferragina S, Migliavacca F, Sala G, et al. Use of rapid prototyping models in the planning of percutaneous pulmonary valved stent implantation. Proceedings of the Institution of Mechanical Engineers, Part H. J Eng Med. 2007;221(4):407–16.

9. Kim MS, Hansgen AR, Wink O, Quaife RA, Carroll JD. Rapid prototyping a new tool in understanding and treating structural heart disease. Circulation. 2008;117(18):2388–94.

10. Wurm G, Tomancok B, Pogady P, Holl K, Trenkler J. Cerebrovascular stereolithographic biomodeling for aneurysm surgery: technical note. J Neurosurg. 2004;100(1):139–45.

11. Giesel FL, Hart AR, Hahn HK, Wignall E, Rengier F, Talanow R, et al. 3D reconstructions of the cerebral ventricles and volume quantification in children with brain malformations. Acad Radiol. 2009;16(5):610–7.

12. Guarino J, Tennyson S, McCain G, Bond L, Shea K, King H. Rapid prototyping technology for surgeries of the pediatric spine and pelvis: benefits analysis. J Pediatr Orthop. 2007;27(8):955–60.

13. Hurson C, Tansey A, O'Donnchadha B, Nicholson P, Rice J, McElwain J. Rapid prototyping in the assessment, classification and preoperative planning of acetabular fractures. Injury. 2007;38(10):1158–62.

14. Hiramatsu H, Yamaguchi H, Nimi S, Ono H. Rapid prototyping of the larynx for laryngeal frame work surgery. Nihon Jibiinkoka Gakkai Kaiho. 2004;107(10):949–55.

15. Winder J, Bibb R. Medical rapid prototyping technologies: state of the art and current limitations for application in oral and maxillofacial surgery. J Oral Maxillofacial Surgery: official journal of the American Association of Oral and Maxillofacial Surgeons. 2005;63(7):1006–15.

16. Fullerton JN, Frodsham GC, Day RM. 3D printing for the many, not the few. Nat Biotechnol. 2014;32(11):1086–7.

17. Hoy MB. 3D printing: making things at the library. Med Ref Serv Q. 2013;32(1):94–9.

18. Choi JW, Kim N. Clinical application of three-dimensional printing technology in craniofacial plastic surgery. Arch Plast Surg. 2015;42(3):267–77.

19. Ventola CL. Medical Applications for 3D Printing: Current and Projected Uses. P T: a peer-reviewed journal for formulary management. 2014;39(10):704–11.

20. Olszewski R, Tranduy K, Reychler H. Innovative procedure for computer-assisted genioplasty: three-dimensional cephalometry, rapid-prototyping model and surgical splint. Int J Oral Maxillofac Surg. 2010;39(7):721–4.

21. Winder J, McRitchie I, McKnight W, Cooke S. Virtual surgical planning and CAD/CAM in the treatment of cranial defects. Stud Health Technol Inform. 2005;111:599–601.

22. Dankowski R, Baszko A, Sutherland M, Firek L, Kalmucki P, Wroblewska K, et al. 3D heart model printing for preparation of percutaneous structural interventions: description of the technology and case report. Kardiol Pol. 2014;72(6):546–51.

23. Rengier F, Mehndiratta A, von Tengg-Kobligk H, Zechmann CM, Unterhinninghofen R, Kauczor HU, et al. 3D printing based on imaging data: review of medical applications. Int J Comput Assist Radiol Surg. 2010;5(4):335–41.

24. McGowan J. 3D printing technology speeds development. Health Estate. 2013;67(9):100–2.

25. Lee H, Fang NX. Micro 3D printing using a digital projector and its application in the study of soft materials mechanics. J Vis Exp: JoVE. 2012;69:e4457.

26. Mironov V, Boland T, Trusk T, Forgacs G, Markwald RR. Organ printing: computer-aided jet-based 3D tissue engineering. Trends Biotechnol. 2003;21(4):157–61.

27. Mankovich NJ, Samson D, Pratt W, Lew D, Beumer 3rd J. Surgical planning using three-dimensional imaging and computer modeling. Otolaryngol Clin North Am. 1994;27(5):875–89.

28. Olszewski Raphael RH. Clinical applications of rapid prototyping models in cranio-maxillofacial surgery. In: Hoque M, editor. Advanced applications of rapid prototyping technology in modern engineering. InTech; 2011. p. 173–206.

29. Choi JY, Choi JH, Kim NK, Kim Y, Lee JK, Kim MK, et al. Analysis of errors in medical rapid prototyping models. Int J Oral Maxillofac Surg. 2002;31(1):23–32.

30. Chang PS, Parker TH, Patrick Jr CW, Miller MJ. The accuracy of stereolithography in planning craniofacial bone replacement. J Craniofac Surg. 2003;14(2):164–70.

31. Schicho K, Figl M, Seemann R, Ewers R, Lambrecht JT, Wagner A, et al. Accuracy of treatment planning based on stereolithography in computer assisted surgery. Med Phys. 2006;33(9):3408–17.

32. Ibrahim D, Broilo TL, Heitz C, de Oliveira MG, de Oliveira HW, Nobre SM, et al. Dimensional error of selective laser sintering, three-dimensional printing and PolyJet models in the reproduction of mandibular anatomy. J Cranio Maxillo Facial Surg: official publication of the European Association for Cranio-Maxillo-Facial Surgery. 2009;37(3):167–73.

33. Silva DN, de Oliveira MG, Meurer E, Meurer MI, da Silva JVL, Santa-Barbara A. Dimensional error in selective laser sintering and 3D-printing of models for craniomaxillary anatomy reconstruction. J Cranio Maxillo Facial Surg: official publication of the European Association for Cranio-Maxillo-Facial Surgery. 2008;36(8):443–9.

34. Ohtani T, Kusumoto N, Wakabayashi K, Yamada S, Nakamura T, Kumazawa Y, et al. Application of haptic device to implant dentistry--accuracy verification of drilling into a pig bone. Dent Mater J. 2009;28(1):75–81.

35. WE L, HE C, editors. Marching cubes: a high resolution 3D surface construction algorithm. ACM siggraph computer graphics. New York: ACM; 1987.

36. Tiede U, Hoehne KH, Bomans M, Pommert A, Riemer M, Wiebecke G. Investigation of medical 3D-rendering algorithms. IEEE Computer Graphics and Applications. 1990;10(2):41–53.

37. Yushkevich PA, Piven J, Hazlett HC, Smith RG, Ho S, Gee JC, et al. User-guided 3D active contour segmentation of anatomical structures: significantly improved efficiency and reliability. Neuroimage. 2006;31(3):1116–28.

38. Shattuck DW, Leahy RM. BrainSuite: an automated cortical surface identification tool. Med Image Anal. 2002;6(2):129–42.

39. Schroeder WJ, Zarge JA, Lorensen WE, editors. Decimation of triangle meshes. ACM Siggraph Computer Graphics. New York: ACM; 1992.

40. Field DA. Laplacian smoothing and Delaunay triangulations. Comm Appl Numer Methods. 1988;4(6):709–12.

41. Hinton E, Campbell J. Local and global smoothing of discontinuous finite element functions using a least squares method. Int J Numer Methods Eng. 1974;8(3):461–80.

42. Mahmood F, Owais K, Taylor C, Montealegre-Gallegos M, Manning W, Matyal R, et al. Three-dimensional printing of mitral valve using echocardiographic data. J Am Coll Cardiol Img. 2015;8(2):227–9.

43. Yang DH, Kang J-W, Kim N, Song J-K, Lee J-W, Lim T-H. Myocardial 3-dimensional printing for septal myectomy guidance in a patient with obstructive hypertrophic cardiomyopathy. Circulation. 2015;132(4):300–1.

44. Jiankang H, Dichen L, Bingheng L, Zhen W, Tao Z. Custom fabrication of composite tibial hemi-knee joint combining CAD/CAE/CAM techniques. Proceedings of the Institution of Mechanical Engineers, Part H. J Eng Med. 2006;220(8):823–30.

45. Wang Z, Teng Y, Li D. Fabrication of custom-made artificial semi-knee joint based on rapid prototyping technique: computer-assisted design and manufacturing. Zhongguo xiu fu chong jian wai ke za zhi= Zhongguo xiufu chongjian waike zazhi= Chinese journal of reparative and reconstructive surgery. 2004;18(5):347–51.

46. Lee M-Y, Chang C-C, Ku Y. New layer-based imaging and rapid prototyping techniques for computer-aided design and manufacture of custom dental restoration. J Med Eng Technol. 2008;32(1):83–90.

47. Dai K-R, Yan M-N, Zhu Z-A, Sun Y-H. Computer-aided custom-made hemipelvic prosthesis used in extensive pelvic lesions. J Arthroplasty. 2007;22(7):981–6.

48. Harrysson OL, Hosni YA, Nayfeh JF. Custom-designed orthopedic implants evaluated using finite element analysis of patient-specific computed tomography data: femoral-component case study. BMC Musculoskelet Disord. 2007;8(1):91.

49. Stevens B, Yang Y, Mohandas A, Stucker B, Nguyen KT. A review of materials, fabrication methods, and strategies used to enhance bone regeneration in engineered bone tissues. J Biomed Mater Res B Appl Biomater. 2008;85(2):573–82.

50. Peltola SM, Melchels FP, Grijpma DW, Kellomäki M. A review of rapid prototyping techniques for tissue engineering purposes. Ann Med. 2008;40(4):268–80.

51. Amerini A, Hatam N, Malasa M, Pott D, Tewarie L, Isfort P, et al. A personalized approach to interventional treatment of tricuspid regurgitation: experiences from an acute animal study. Interact Cardiovasc Thorac Surg. 2014;19(3):414–8.

52. Griffith LG, Naughton G. Tissue engineering--current challenges and expanding opportunities. Science (New York, NY). 2002;295(5557):1009–14.

53. Melchels FP, Domingos MA, Klein TJ, Malda J, Bartolo PJ, Hutmacher DW. Additive manufacturing of tissues and organs. Prog Polym Sci. 2012;37(8):1079–104.

54. Murphy SV, Atala A. 3D bioprinting of tissues and organs. Nat Biotechnol. 2014;32(8):773–85.

55. Huh D, Matthews BD, Mammoto A, Montoya-Zavala M, Hsin HY, Ingber DE. Reconstituting organ-level lung functions on a chip. Science (New York, NY). 2010;328(5986):1662–8.

56. Huh D, Hamilton GA, Ingber DE. From 3D cell culture to organs-on-chips. Trends Cell Biol. 2011;21(12):745–54.

57. Shim JH, Jang KM, Hahn SK, Park JY, Jung H, Oh K, et al. Three-dimensional bioprinting of multilayered constructs containing human mesenchymal stromal cells for osteochondral tissue regeneration in the rabbit knee joint. Biofabrication. 2016;8(1):014102.

58. Lewis PL, Shah RN. 3D printing for liver tissue engineering: current Approaches and future challenges. Curr Transpl Reports. 2016;3(1):100–8.

59. Maeshima A, Takahashi S, Nakasatomi M, Nojima Y. Diverse cell populations involved in regeneration of renal tubular epithelium following acute kidney injury. Stem Cells Int. 2015;2015:964849.

60. Moon KH, Ko IK, Yoo JJ, Atala A. Kidney diseases and tissue engineering. Methods. 2016;99:112–9.

61. Ohashi K, Okano T. Functional tissue engineering of the liver and islets. Anat Rec. 2014;297(1):73–82.

62. Scarritt ME, Pashos NC, Bunnell BA. A review of cellularization strategies for tissue engineering of whole organs. Front Bioeng Biotechnol. 2015;3:43.

63. Price AP, Godin LM, Domek A, Cotter T, D'Cunha J, Taylor DA, et al. Automated decellularization of intact, human-sized lungs for tissue engineering. Tissue Eng Part C Methods. 2015;21(1):94–103.

64. Bueno EM, Diaz-Siso JR, Sisk GC, Chandawarkar A, Kiwanuka H, Lamparello B, et al. Vascularized composite allotransplantation and tissue engineering. J Craniofac Surg. 2013;24(1):256–63.

65. Sears NA, Dhavalikar PS, Seshadri D, Cosgriff-Hernandez E. A review of 3D printing of tissue engineering constructs. Tissue Eng Part B Rev. 2016;22(4):298–310.

66. Rodriguez-Devora JI, Zhang B, Reyna D, Shi ZD, Xu T. High throughput miniature drug-screening platform using bioprinting technology. Biofabrication. 2012;4(3):035001.

67. Hendriks J, Willem Visser C, Henke S, Leijten J, Saris DB, Sun C, et al. Optimizing cell viability in droplet-based cell deposition. Sci Rep. 2015;5:11304.

68. Gao G, Cui X. Three-dimensional bioprinting in tissue engineering and regenerative medicine. Biotechnol Lett. 2016;38(2):203–11.

69. Wu Z, Su X, Xu Y, Kong B, Sun W, Mi S. Bioprinting three-dimensional cell-laden tissue constructs with controllable degradation. Sci Rep. 2016;6:24474.

70. Pati F, Jang J, Ha DH, Won Kim S, Rhie JW, Shim JH, et al. Printing three-dimensional tissue analogues with decellularized extracellular matrix bioink. Nat Commun. 2014;5:3935.

71. Ozbolat IT, Hospodiuk M. Current advances and future perspectives in extrusion-based bioprinting. Biomaterials. 2016;76:321–43.

72. Duan B. State-of-the-art review of 3D bioprinting for cardiovascular tissue engineering. Ann Biomed Eng. 2016, in press.

73. Skardal A, Devarasetty M, Kang HW, Mead I, Bishop C, Shupe T, et al. A hydrogel bioink toolkit for mimicking native tissue biochemical and mechanical properties in bioprinted tissue constructs. Acta Biomater. 2015;25:24–34.

74. Stanton MM, Samitier J, Sanchez S. Bioprinting of 3D hydrogels. Lab Chip. 2015;15(15):3111–5.

75. Chua CK, Yeong WY. Materials for bioprinting. In: Bioprinting: principles and applications. Singapore: World Scientific Publishing Co. Pte. Ltd.; 2014. p. 117–64.

76. Ozbolat IT, Yu Y. Bioprinting toward organ fabrication: challenges and future trends. IEEE Trans Biomed Eng. 2013;60(3):691–9.

77. Murphy SV, Atala A. 3D bioprinting of tissues and organs. Nat Biotechnol. 2014;32(8):773–85.

78. Kang H-W, Lee SJ, Ko IK, Kengla C, Yoo JJ, Atala A. A 3D bioprinting system to produce human-scale

tissue constructs with structural integrity. Nat Biotechnol. 2016;34(3):312–9.

79. Luiz EB, Juliana CC, Vijayan M, Ana LC, Nupura SB, Wesleyan AA, et al. Direct-write bioprinting of cell-laden methacrylated gelatin hydrogels. Biofabrication. 2014;6(2):024105.

80. Skardal A, Zhang J, Prestwich GD. Bioprinting vessel-like constructs using hyaluronan hydrogels crosslinked with tetrahedral polyethylene glycol tetracrylates. Biomaterials. 2010;31(24):6173–81.

81. Kolesky DB, Homan KA, Skylar-Scott MA, Lewis JA. Three-dimensional bioprinting of thick vascularized tissues. Proc Natl Acad Sci U S A. 2016;113(12):3179–84.

82. Holmberg KV, Hoffman MP. Anatomy, biogenesis and regeneration of salivary glands. Monogr Oral Sci. 2014;24:1–13.

83. Jakab K, Norotte C, Marga F, Murphy K, Vunjak-Novakovic G, Forgacs G. Tissue engineering by self-assembly and bio-printing of living cells. Biofabrication. 2010;2(2):022001.

84. Chan YH, Huang TW, Young TH, Lou PJ. Human salivary gland acinar cells spontaneously form three-dimensional structures and change the protein expression patterns. J Cell Physiol. 2011;226(11): 3076–85.

85. Joraku A, Sullivan CA, Yoo J, Atala A. In-vitro reconstitution of three-dimensional human salivary gland tissue structures. Differentiation. 2007;75(4):318–24.

86. Maria OM, Maria O, Liu Y, Komarova SV, Tran SD. Matrigel improves functional properties of human submandibular salivary gland cell line. Int J Biochem Cell Biol. 2011;43(4):622–31.

87. Mandrycky C, Wang Z, Kim K, Kim DH. 3D bioprinting for engineering complex tissues. Biotechnol Adv. 2016;34(4):422–34.

88. Jeong GS, Song JH, Kang AR, Jun Y, Kim JH, Chang JY, et al. Surface tension-mediated, concave-microwell arrays for large-scale, simultaneous production of homogeneously sized embryoid bodies. Adv Healthc Mater. 2013;2(1):119–25.